# Growth mechanisms of coevaporated $SmBa_2Cu_3O_y$ thin films

B. Stäuble-Pümpin, V. C. Matijasevic, B. Ilge, J. E. Mooij, W. J. A. M. Peterse, P. M. L. O. Scholte, F. Tuinstra, H. J. Venvik,* and D. S. Wai
*Department of Applied Physics, Solid State Physics, TU Delft, Lorentzweg 1, 2628 CJ Delft, The Netherlands*

C. Træholt, J. G. Wen,† and H. W. Zandbergen
*Centre for HREM, Laboratory of Material Science, TU Delft, Rotterdamseweg 137, 2628 AL Delft, The Netherlands*
(Received 27 March 1995)

The growth mechanisms of coevaporated $SmBa_2Cu_3O_y$ (Sm123) films grown epitaxially on ⟨100⟩ $SrTiO_3$ substrates were investigated using scanning probe microscopy, transmission electron microscopy, scanning electron microscopy, and x-ray diffraction. The Sm123 films were predominantly oriented with their crystallographic $c$ axis perpendicular ($c\perp$) to the substrate. Only small fractions of grains with their $c$ axis parallel to the substrate ($c\parallel$) and some impurity phases were found. It was found that Sm123 growing with a $c\perp$ orientation displayed a frequent bending of its unit-cell thick layers, which could often be related to the presence of impurity phases. We present strong evidence that this impurity-related bending of the Sm123 lattice is responsible for the formation of screw dislocations. Furthermore, we find that the volume fraction of $c\parallel$ to $c\perp$ material increases with increasing chamber pressure and decreasing substrate temperature, indicating that kinetic factors (i.e., reduced mobility of the adsorbed species during film growth) play an important role for the formation and growth of $c\parallel$ grains. No evidence for a strain-driven crossover from $c\perp$ to $c\parallel$ growth as a function of film thickness was found. It was also observed that the presence of $c\parallel$ outgrowths depends on the amount of CuO droplets on the surface of the films. This suggests that impurity phases can play a role in the formation of $c\parallel$ grains. Finally, many of the impurity phases observed in our films are unexpected from a thermodynamic point of view, suggesting that the kinetic barrier to their creation is low. Based on the results presented here, the smoothest and most homogeneous $RBa_2Cu_3O_y$ ($R$ = Y or lanthanide) films are expected to grow under conditions which favor a high surface mobility during film growth.

## I. INTRODUCTION

In recent years, a considerable effort has been aimed at growing uniform films of the high-temperature superconductor $RBa_2Cu_3O_y$ ($R$ = Y or lanthanide, $y \cong 7$). A large number of studies have been published stating under which growth conditions the best films were processed.[1] However, the various results are very often not correlated, which is probably due to the large variety of deposition techniques and parameters involved: pulsed versus continuous deposition, evaporation from single or multiple sources, use of molecular oxygen, atomic oxygen or ozone, presence of highly energetic particles, use of different types of substrates, etc. For this reason, the study presented here will not try to give a "recipe" of how to grow qualitatively good cuprate films. Instead its aim is to focus on the basic mechanisms underlying the growth of the investigated films, in this case $SmBa_2Cu_3O_y$ (Sm123). In particular, the influence of kinetic factors on the morphology of the deposited films will be examined. Up to a certain extent, it should be possible to extrapolate the results obtained in this study to other $RBa_2Cu_3O_y$ ($R$ = Y or lanthanide) films grown with other techniques and under different conditions than those described here.

The details of film fabrication are described in Sec. II. Section III gives an overview of the experimental techniques used to characterize these films. These techniques were scanning electron microscopy (SEM), scanning tunneling microscopy (STM), atomic force microscopy (AFM), transmission electron microscopy (TEM), and x-ray diffraction (XRD). It was found that the structures typically present in the Sm123 films can be classified into three categories: Sm123 growing with its crystallographic $c$ axis perpendicular to the substrate (Sec. IV), Sm123 growing with its crystallographic $c$ axis parallel to the substrate (Sec. V), and impurity phases (Sec. VI). Conclusions are given in Sec. VII.

## II. FILM FABRICATION

The films studied here were made by coevaporation in a molecular beam epitaxy system adapted for deposition of oxides. Details of the system can be found in Refs. 2–4. The system is equipped with four Knudsen cells ($K$ cells) and two electron guns which are independently shuttered. All the films presented here were grown by codeposition. The calibration is done by opening each of the source shutters independently prior to deposition, and measuring the deposition rate of the oxide with a quartz crystal microbalance placed in the sample position. The individual source rates are then adjusted for the desired metal-atom stoichiometry. The relative stability of the sources is 1–2 % per hour.[2] Cu is deposited from an electron gun, while Ba and Sm are evaporated from $K$ cells. Samarium sublimes at a relatively low tem-

0163-1829/95/52(10)/7604(15)/$06.00  

perature (below 700 °C), which was the initial reason for choosing Sm over Y in the "123" compound. In order to oxidize copper and provide conditions for stability of the "123" compound, we use an ozone beam at the growth surface. The ozone incidence rate is approximately $10^{16}$ mol $s^{-1}$ $cm^{-2}$. The proximity of the ozone tubes to the substrate and the large pumping speed (3000 1/s) produce a differential pumping within the system. The background pressure in the vacuum chamber is $3-5\times10^{-6}$ mbar. As the pumping speed of the system remains constant in our range of pressures, any change in the background pressure (also called chamber pressure in what follows) is directly proportional to a change in the ozone incidence rate.

All the films discussed here were grown on ⟨100⟩ $SrTiO_3$ substrates, $5\times5\times1$ $mm^3$ with one side polished.[5] The substrates were cleaned by ultrasonic agitation in organic solvents. In addition, just prior to deposition, the substrates were heated to 850 °C in the ozone beam, inside the vacuum deposition system.

The growth of the Sm123 films was optimized in terms of their critical temperature $T_c$ and their transport properties.[2,3] In order to obtain films with a $T_c$ above 90 K, it was necessary to use substrate temperatures, $T_{sub}$ above 750 °C, significantly (100 °C) higher than the temperatures required for $YBa_2Cu_3O_y$ (Y123). As shown in Refs. 2 and 3, films grown under these conditions are predominantly $c$-axis oriented, i.e., with their crystallographic $c$ axis perpendicular to the substrate. When measured, the critical temperature $T_c$ was always around 92–93 K. Typically, the critical current for films grown under the conditions described here is $\geq 10^6$ A/$cm^2$ at 77 K.

Transmission electron microscopy (TEM) cross-sectional studies of Y123 films on $SrTiO_3$ substrates showed that, in general, in a $c$-axis oriented Y123 film, the BaO layer corresponds to the first atomic layer next to the substrate.[6] Furthermore it is known that deposition of excess Cu in the early stages of growth creates $Cu_2O$ grains[7,8] which grow steadily regardless of the changes in the composition thereafter. For these reasons we have chosen to grow our films in such a way as to start the deposition process by opening the shutters in the following sequence: Ba, Sm, Cu. The time between the openings is equivalent to depositing a monolayer of each of the oxides. In order to preserve the total composition for the film, we repeated the procedure for closing the shutters at the end of the deposition process, i.e., closing sequence: Ba, Sm, Cu. This was the only independent "shuttering" done in the growth process.

Obviously, a large number of variables can influence nucleation and growth during film deposition. We have attempted to keep as many of them constant as possible by fixing the deposition parameters over which we do have control. The total growth rate was kept at 0.1–0.2 nm/s. The thickness of all the films described here is 150 nm. The substrates were always ⟨100⟩ $SrTiO_3$, but the surface miscut, or vicinal, angle was varied. The parameters that were varied independently are composition, vicinal angle, substrate temperature, and ozone flux (chamber pressure). A list of all investigated films and the conditions under which they were deposited is given in Table I.

## III. EXPERIMENTAL TECHNIQUES

In order to obtain a comprehensive picture of the nanostructures present in the Sm123 films, a variety of experimental techniques were applied to characterize them. Local information on the surface structure of the films was obtained by means of SEM (scanning electron microscopy), STM (scanning tunneling microscopy) and AFM (atomic force microscopy). Scanning electron mi-

TABLE I. List of Sm123 films with the corresponding substrate temperature $T_{sub}$ and chamber pressure $p$ during deposition, vicinal angle $\alpha$ of the $SrTiO_3$ substrate, and Sm, Ba, and Cu contents in percentage of the total amount of deposited metal ions. The first row of the table ("123") gives the Sm, Ba, and Cu contents of an ideal film grown on stoichiometry (n.m. represents not measured).

| Film | $T_{sub}$ (°C) | $p$ (mbar) | $\alpha$ (deg) | Sm (%) | Ba (%) | Cu (%) |
|---|---|---|---|---|---|---|
| "123" | | | | 16.6 | 33.3 | 50 |
| GS | 825(10) | $3\times10^{-5}$ | 0.15(5) | 17(1) | 32(1) | 51(1) |
| GR | 800 | $3\times10^{-5}$ | n.m. | 17 | 33 | 51 |
| GV | 800 | $5\times10^{-6}$ | n.m. | 17 | 32 | 51 |
| HB | 800 | $5\times10^{-6}$ | 0.65 | 18 | 34 | 47 |
| HI | 800 | $5\times10^{-6}$ | n.m. | 21 | 33 | 46 |
| HL | 800 | $5\times10^{-6}$ | 0.75 | 19 | 32 | 49 |
| HM | 800 | $5\times10^{-6}$ | 0.85 | 19 | 32 | 49 |
| HN | 800 | $2\times10^{-6}$ | n.m. | 17 | 34 | 50 |
| HR | 800 | $5\times10^{-6}$ | 0.65 | 21 | 31 | 48 |
| HV | 780 | $5\times10^{-6}$ | 0.35 | 18 | 33 | 48 |
| II | 700 | $5\times10^{-6}$ | 0.45 | 19 | 31 | 50 |
| IR | 790 | $5\times10^{-6}$ | 0.25 | 19 | 34 | 47 |
| IX | 790 | $5\times10^{-6}$ | 0.35 | 18 | 34 | 47 |
| JY | 800 | $5\times10^{-6}$ | 0.97 | 16 | 32 | 52 |
| KA | 750 | $5\times10^{-6}$ | 0.40 | 19 | 34 | 47 |

crographs were taken with a JEOL JSM840 system at a tilt angle of approximately 30°. The measurements were typically performed with an acceleration voltage of 25 kV and a current between $10^{-10}$ and $10^{-11}$ A. STM measurements were performed with a commercially available instrument [Nanoscope II (Ref. 9)]. The STM images were all acquired in the constant current mode using mechanically sharpened PtIr tips. Sample bias voltages were typically 750 mV and set-point currents 100 pA. Additional images were obtained on a commercially available AFM [Nanoscope III (Ref. 9)]. The measurements were performed in the tapping mode with Si-type cantilevers.

Further information on a nanometer scale was obtained by looking at the cross sections of Sm123 films by means of TEM and HREM (high-resolution electron microscopy). A detailed description of the method used to prepare cross-section specimens is given in Ref. 10. Electron microscopy was performed with a Philips CM30ST electron microscope (operated at 300 kV) equipped with a field emission gun and a Link EDX element analysis system.

Finally, x-ray diffraction (XRD) measurements provided global information (i.e., averaged over a large volume) on the structures present in Sm123 films. The results presented here were obtained from rocking curves ($\omega$ scans) measured with a standard four-circle diffractometer. A 10-kW rotating anode generator with a copper target was used as an x-ray source. The beam (with a Cu $K\alpha$ wavelength of 1.540 51 Å) was first monochromized by a Ge(220) Bragg reflection and then collimated. The wave-vector resolution in the scattering plane was of the order of $3.5\times10^{-3}$ Å$^{-1}$. A NaI(TI) scintillation counter was used as a detector.

## IV. Sm123 GROWING WITH THE *c*-AXIS PERPENDICULAR TO THE SUBSTRATE

### A. Short review of growth models

#### *1. Step flow growth versus island growth*

Based on previous work on coevaporated Sm123 films,[2,3] the films investigated in this study were deposited under conditions where *c*-axis-oriented films are expected to grow. X-ray-diffraction measurements, to be described in more detail later, confirm that large fractions of the Sm123 material (typically 92–100 %) have the desired orientation. When investigated on a nanometer scale by means of STM and/or AFM, the surfaces of these films are found to be characterized by two rather different types of topographies. The surfaces of films grown at higher substrate temperatures $T_{sub}$ ($T_{sub}\geq800$ °C) on substrates with larger vicinal angles ($\alpha=0.65°-0.97°$) are characterized by a seemingly infinite superposition of terraces, as seen in Fig. 1(a). On the other hand, films grown at somewhat lower substrate temperatures ($T_{sub}<800$ °C) and lower vicinal angles ($\alpha=0.10°-0.45°$) display a surface structure best described by the growth of three-dimensional islands having the shape of spirals [see Fig. 1(b)]. For both types of surface topography, AFM and STM data revealed that whenever tip artifacts could be excluded, the step height between two adjacent terraces was equal to the lattice parameter *c* of Sm123 (or a multiple of it). These observations are consistent with a detailed study by Schlom *et al.*,[11] where the density of screw-dislocation mediated spirals $\rho_{screw}$ on sputtered $YBa_2Cu_3O_y$ (Y123) films was found to decrease with increasing substrate temperature and/or vicinal angle. As suggested in Refs. 11 and 12, most of these features can be qualitatively understood by comparing the terrace width $L_T$ between adjacent steps and the surface diffusion length $L_D$ during film deposition.

It is clear that the value of the terrace width $L_T$ on the surface of the substrate is related to the vicinal (or miscut) angle $\alpha$ of the substrate by means of the equation

$$L_T=a\cot\alpha\ , \tag{1}$$

where the step height $a$ is equal to the lattice parameter

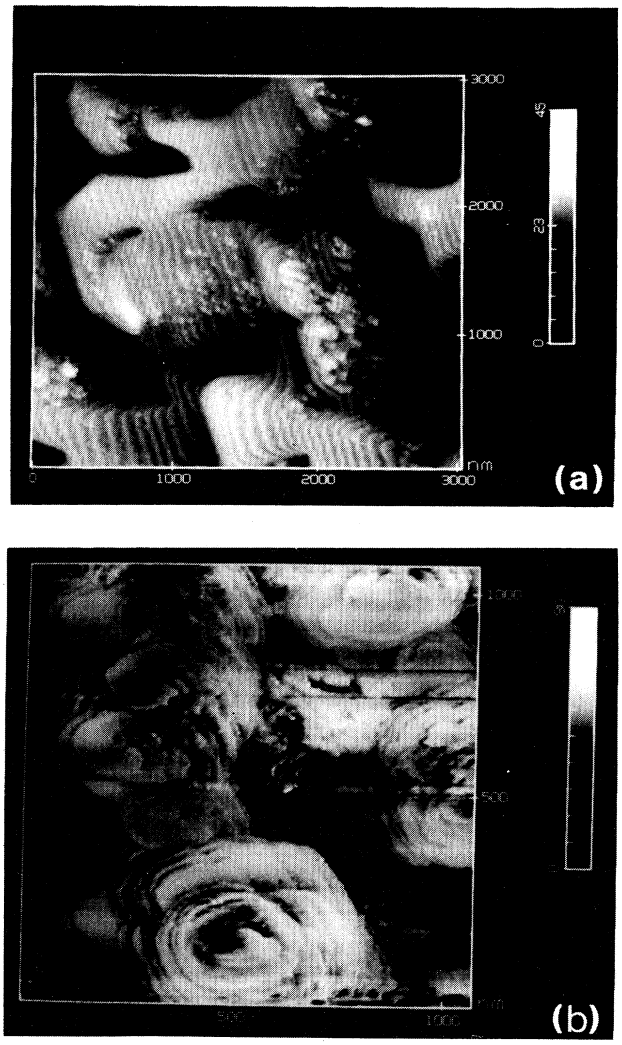


FIG. 1. STM images of coevaporated Sm123 films grown on $SrTiO_3$ showing a surface morphology characterized by (a) an apparently infinite superposition of terraces (film JY, see Table I) and (b) spiral-shaped islands (film IX).

of $SrTiO_3$ (=3.905 Å). As an example, an AFM micrograph of the surface of a $SrTiO_3$ substrate is shown in Fig. 2. The mean distance between adjacent steps on this image is $L_T=85(5)$ nm. From independent XRD measurements, the vicinal angle of this same substrate was found to be equal to 0.27(5)°. Using Eq. (1), this yields a step length of 83(15) nm, which is in excellent agreement with the AFM results.

The surface diffusion length $L_D$ can be understood as the mean length traveled by an atom or a molecule (to be called species in what follows) on the surface of the film, before being incorporated into the bulk of the film either by formation of a nucleation island together with other species or by incorporation at a growth front. Note that for the growth of our Sm123 films, we have experimental evidence indicating that none of the metallic species are desorbed from the surface of the growing film (a sticking coefficient of 1 is observed).[2,3] It seems probable that, because of the reactiveness of ozone, the metal atoms form oxide molecules which diffuse on the surface of our films. In the case of Sm (which sublimes at approximately 700 °C, see Sec. II) this would explain why a sticking coefficient of 1 is measured, even for films grown at 800 °C. The diffusion length $L_D$, which reflects the surface mobility of the diffusing species, will decrease if the growth rate is increased (i.e., increase in the partial pressure of the metallic species), the chamber pressure is increased (i.e., increase in ozone flux) and/or the substrate temperature is decreased.

Step edges act as preferential adsorption sites for atoms diffusing on the surface of the substrate. Therefore, different types of film nucleation and growth are expected depending on the relative size of $L_T$ and $L_D$. For instance, if the diffusion length $L_D$ is much larger than the terrace width $L_T$ (i.e., for large $T_{sub}$ and/or $\alpha$), one unit-cell high grains will nucleate at the substrate steps. In this case, growth will continue by incorporating material at the step edges, a process called step-flow growth. On the other hand, if the diffusion length $L_D$ is much smaller than the terrace width $L_T$ (i.e., for small $T_{sub}$ and/or $\alpha$), islands will nucleate away from the terrace steps. More details on the nucleation mechanisms of Sm123 films are given in Ref. 13, where ultrathin Sm123 films (nominally 0.33, 0.75, and 1 unit cell thick) grown on vicinal $SrTiO_3$ substrates were investigated using AFM.

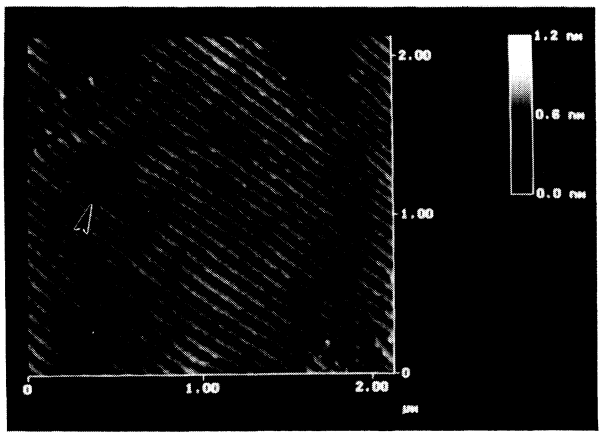


FIG. 2. AFM image of a $SrTiO_3$ substrate. The arrow points at a (screw) dislocation.

Although this simple model can qualitatively describe the early stages of film nucleation and growth, it fails to predict the features observed on thicker films. In particular, it cannot explain the large densities of spiral-shaped islands observed on most Y123 films. Spirals are known to be produced by the intersection of a dislocation (of screw or mixed character) with the surface of the film. The origin of these dislocations is at present unclear.

### 2. *Formation of screw dislocations*

A number of possible mechanisms for the formation of screw dislocations in Y123 films have been examined in literature. They are the following.

(1) Inheritance from the substrate.[11] It seems unlikely that this is the only operating mechanism since the density of screw dislocations observed by means of AFM on the surface of $SrTiO_3$ substrates was found to be equal to $10^8$ $cm^{-2}$ or less (see, e.g., Refs. 11 and 14). This is 1–2 orders of magnitude smaller than the densities usually observed on Y123 and related films (see, e.g., Ref. 11).

(2) Meeting of misaligned growth fronts.[11,12,15,16] Growth fronts meet, for instance, as the nucleation islands coalesce or when two separate branches of the same initial growth front recombine. From TEM,[17–19] it is known that some Y123 nucleation islands do grow rotationally misaligned on MgO substrates. This misalignment is attributed to the large lattice mismatch between MgO and Y123. Pennycook *et al.*[12] suggest that when these misaligned nucleation islands coalesce, screw dislocations are likely to be formed. However, a misalignment of growth fronts which is purely rotational will result in a dislocation with a Burgers vector in the plane of the substrate, and can therefore not be responsible for the spiral growth observed on Y123 films. The smallest Burgers vector **b** required for the growth of spiral-shaped islands on *c*-axis-oriented Y123 and related films is equal to **b**=[001]. In other words, if the generation of screw dislocations results from the meeting of misaligned growth fronts, a vertical misalignment by one lattice constant *c* (i.e., approximately 12 Å) is needed.

(3) Release of strain by formation of dislocation half-loops.[12] Due to the lattice mismatch between substrate and film, Y123 grows strained on $SrTiO_3$. As the film grows thicker, the elastic strain energy increases. At a critical thickness, however, the energy needed to form a dislocation in the lattice is less than the elastic energy it relaxes. A typical way of introducing strain-releasing defects into a film is by formation of dislocation half-loops at the surface of the film which then glide to the interface with the substrate. It has been proposed[12] that such dislocation half-loops could be responsible for both spiral growth and strain release. Note that this would require dislocations of mixed type, i.e., with an edge component at the interface (to release the strain) and a screw component at the surface of the film (to mediate spiral growth). In Y123, this would result in a very long and

energetically unfavorable Burgers vector **b**.[16] [From isotropic dislocation theory, it is known that the self-energy per unit length of a dislocation line consists of a core term and a long-range term which is proportional to $b^2$. In addition, the activation energy required for the formation of a dislocation half-loop is proportional to $b^3$.[20] Within this theory, the activation energy to form a dislocation loop with **b**=[101] in Y123 (approximately 900 eV) is not physically attainable at the temperatures at which these films are typically grown.[20–22] Of course, anisotropic dislocation theory would provide more accurate results.]

A satisfactory explanation for the formation of screw dislocations in Y123 and related films still remains elusive. While it is mostly accepted that the first of the discussed models ("inheritance of screw dislocations from the substrate") is unlikely to be the only operating mechanism, it remains open whether the "misaligned growth front," the "dislocation half-loop," or some other mechanism is responsible for the large densities of screw dislocations in Y123 films.

### B. Experimental results

In the past years, several comprehensive studies on films displaying spiral growth have been published.[11,12,16,23–31] However, only limited information is available on films grown in the step-flow mode. Therefore, to gain new insights into the growth mechanisms of $RBa_2Cu_3O_y$ ($R$ = Y or lanthanide) films on $SrTiO_3$ substrates, the study presented here focused on Sm123 films which do not display spiral-shaped islands on their surface. It should be emphasized that, although spiral-shaped islands are absent from the surface of these films, screw dislocations (which refer to a line of defects in the solid) can nevertheless be present.

The investigated films were deposited at high substrate temperatures (typically 800 °C) on substrates with relatively large miscuts (vicinal angle $\alpha = 0.65-0.97°$), i.e., under conditions where step-flow growth is expected. Note that the Sm-based superconductor grown in this study is particularly adequate for investigating step-flow growth since good quality Sm123 films are obtained at significantly higher substrate temperatures than comparable Y123 films (see also Sec. II, film fabrication). The miscut angle of the substrate was determined by optically aligning the sample with a laser and then measuring the position of two different crystal reflections using a standard four-circle diffractometer [in general the (002) reflection of $SrTiO_3$ and the (104) reflection of Sm123]. The angles $\alpha$ and $\beta$ used to characterize the direction of the surface normal $N_{surf}$ with respect to the crystal lattice are schematically represented in Fig. 3.

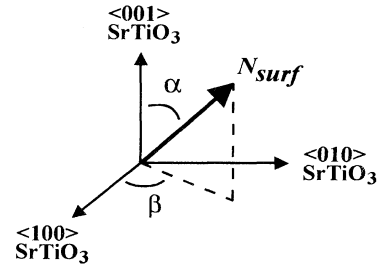


FIG. 3. Schematic representation of the angles $\alpha$ and $\beta$ characterizing the miscut of the substrate. $N_{surf}$ is the normal to the optical surface of the substrate.

#### 1. Scanning tunneling microscopy

A STM image of a film deposited on a substrate with a miscut angle $\alpha = 0.97(5)°$ at a substrate temperature $T_{sub} = 800(10)$ °C (film JY, see Table I) is displayed in Fig. 4(a). It shows the characteristic stack of terraces resulting from the step-flow growth. The height difference be-

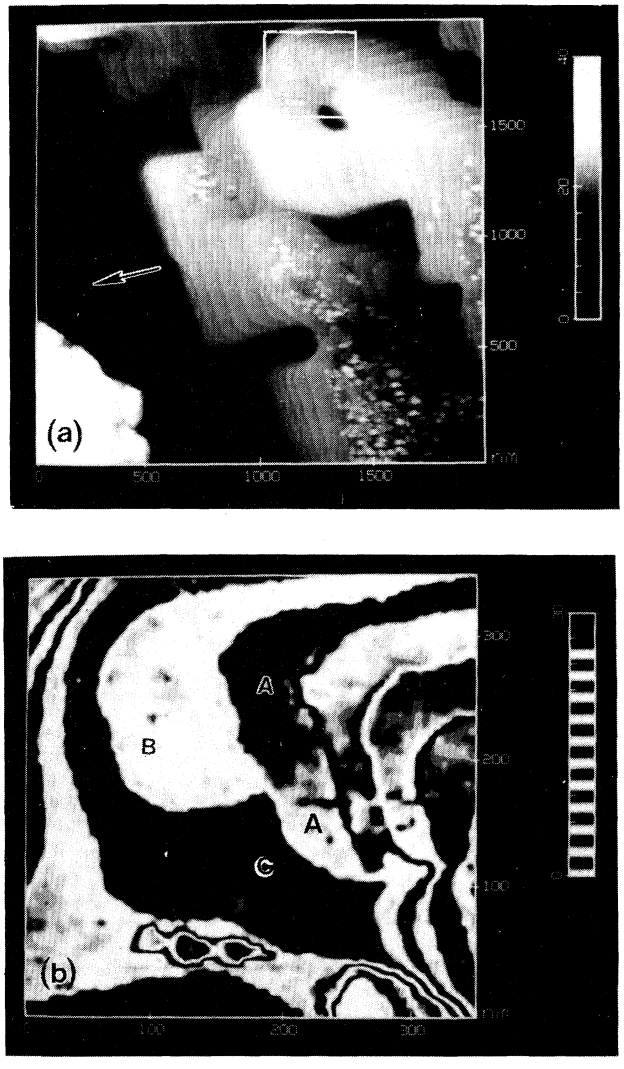


FIG. 4. (a) Typical STM image of a coevaporated Sm123 film (sample JY, see Table I) grown in the step-flow mode. The arrow roughly shows the direction toward which the substrate is miscut (see text for more details). (b) Enlarged area of (a) showing a unit-cell thick layer of Sm123 (layer $A$) bending over two other unit-cell thick layers of the same material (layers $B$ and $C$). The grey scale in the $z$ direction was chosen to emphasize the tilting of layer $A$.

tween two terraces is typically equal to one lattice parameter $c$, while the mean terrace length $L_T$ is 66(2) nm (averaged over a large number of different STM images). Using Eq. (1), this yields an angle $\alpha_{123}=1.04(3)°$, comparable to the miscut angle $\alpha=0.97(5)°$ of the substrate. Although this is consistent with a constant thickness of the Sm123 film, it also means that the mean terrace length of Sm123 is three times larger than the mean terrace length of the underlying substrate [see Eq. (1)]. The mechanism leading to these changes in terrace length will be discussed later in this section (see *transmission electron microscopy*).

For this particular film (JY), the miscut angle $\beta$ is rather small [$\beta=13(10)°$], i.e., the normal to the surface $N_{surf}$ practically lies within the (010) plane of the substrate (see Fig. 3). The near alignment of the $N_{surf}$ with the (010) planes allows us to represent the vicinal steps as essentially lying along the ⟨010⟩ direction. This rather simple model is justified by AFM images of the surface of miscut $SrTiO_3$ substrates (see, e.g., Fig. 2), where the step edges are all observed to run along the same direction. The arrow in Fig. 4(a) roughly represents the projection of $N_{surf}$ onto the crystallographic (001) planes of the film.

An interesting feature of the surface in Fig. 4(a) is that the flow of growth fronts during film deposition appears to have been delayed at certain points. This results in narrow "valleys" which are in general rather deep (of the order of 20 unit cells, i.e., approximately 24 nm) and display large slopes perpendicular to the flow direction, typically 10°–20° or more (the resolution being determined by the sharpness of the STM tip). For comparison, the slopes of screw-dislocation-mediated spirals usually lie between 0.7° and 1.2° (see, e.g., Refs. 11, 29, and 30). The pinning of advancing growth fronts occurs most probably at second phases. A possible explanation for the considerable depth of the valleys is provided by the high density of favorable adsorption sites (i.e., step edges) along the large slopes of these valleys. As a consequence, the probability for an incoming atom (or oxide) to reach the bottom of a valley is small.

In some cases the different branches of a pinned growth front recombine behind the impurity responsible for the pinning, transforming the valleys into "holes" (see Fig. 5). From careful height measurements, it is known that all the numbered terraces in Fig. 5 have a step height corresponding to only one lattice parameter $c$ of Sm123. Nevertheless, a different number of terraces is counted on the two sides of the hole, indicating the presence of a dislocation. In the case of Fig. 5, the Burgers vector associated to this dislocation is equal to twice the lattice parameter $c$. The presence of dislocations in the proximity of a hole has repeatedly been observed on our films. A possible model for this will be discussed in Sec. IV C.

Another characteristic feature of the surfaces investigated here is a frequent "bending" of unit-cell thick layers of Sm123. As an example, Fig. 4(b) shows an enlarged area of Fig. 4(a), where a unit-cell thick layer of Sm123 (layer $A$) is observed to have grown over two other unit-cell thick layers of the same material (layers $B$ and $C$). The unusual gray scale in the $z$ direction was chosen to emphasize the characteristic tilting of layer $A$. The elastic energy associated to the tilt shown in Fig. 4(b) can be estimated from the equation

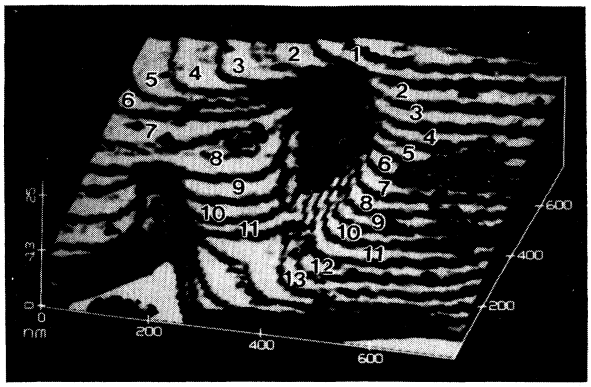


FIG. 5. STM micrograph of a Sm123 film growth in the step-flow mode (film JY, see Table I). Note that the amount of numbered terraces, all unit-cell high, is different on the left and right side of the "hole."

$$W=(C_{44}\varepsilon^2)/2\ , \tag{2}$$

where $C_{44}=61$ GPa (Ref. 21) is the elastic-stiffness constant (shear modulus) of Y123 and $\varepsilon$ represent the elastic strain of the bended layer (see also Ref. 32). For layer $A$ in Fig. 4(b), this strain is approximately equal to 0.03, yielding an elastic energy of the order of 30 meV per unit cell of Sm123. For comparison, the thermal energy available during film growth is equal to $k_B T_{sub}=92$ meV.

Because of the small values of the elastic-stiffness constants $C_{44}$ (and $C_{55}$) in this perovskite-type structure, the elastic energy related to the bending of a Sm123 layer is small too. This explains why structures comparable to the one shown in Fig. 4(b) were frequently observed on the surfaces of our films.

### 2. *Transmission electron microscopy*

Additional information on the growth of Sm123 films was obtained from cross-sectional TEM analysis. Figure 6 displays cross sections of the film whose surface is shown in Figs. 4 and 5 (film JY). The TEM sample was cut parallel to the miscut direction of the substrate. As mentioned earlier in this section, the miscut for film JY lies practically within the crystallographic (010) planes, which facilitates the imaging of steps in the substrate.

Figure 6(a) displays a cross-sectional view of the film-substrate interface, showing a series of steps in the $SrTiO_3$ substrate (see arrows). The length of the steps in the substrate is approximately 24 nm, in agreement with the vicinal angle of the substrate [$\alpha=0.97(5)°$, from x-ray diffraction]. TEM imaging reveals that the presence of steps in the substrate usually results in the formation of antiphase boundaries [see Fig. 6(a)], which can be slightly shifted with regard to the position of the step edge. In general, these antiphase boundaries "heal out" after a few (typically 5) unit cells from the interface by inclusion of planar defects. A consequence of this "healing" is that the length of Sm123 terraces becomes three

times larger than the length of the $SrTiO_3$ terraces, in agreement with the STM results presented earlier.

In addition, the Burgers path displayed in Fig. 6(a) (dotted line) reveals the existence of a Burgers vector with $\mathbf{b}=[001]$. Although several mechanisms could explain the formation of such a defect in the Sm123 lattice, it should be pointed out that a cross section through the "bended" Sm123 layer of Fig. 4(b) would eventually be comparable to what is observed in Fig. 6(a).

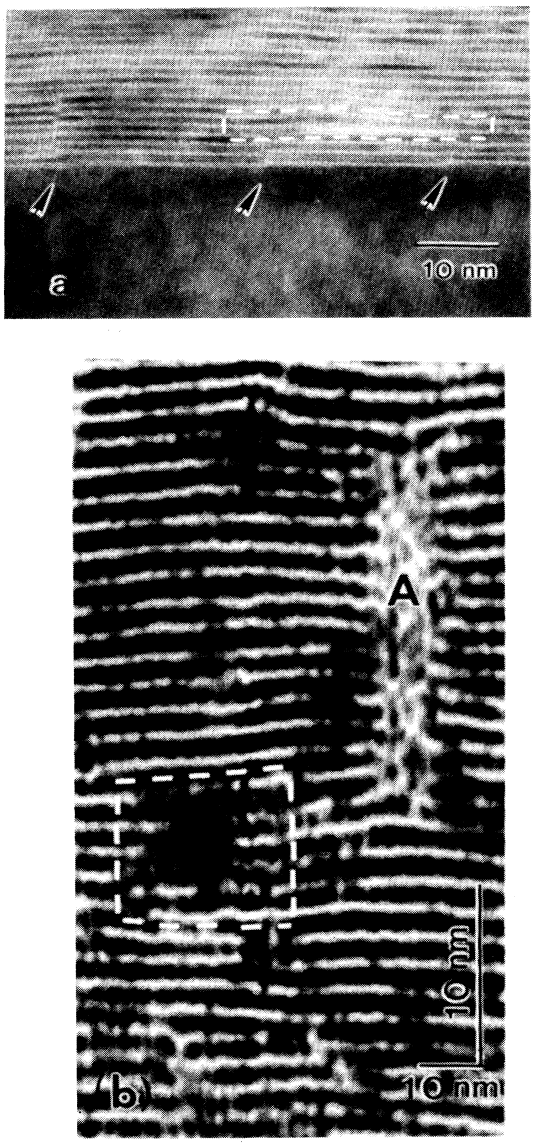


FIG. 6. TEM cross-sectional view of the Sm123 film whose surface is shown in Figs. 4 and 5 (film JY, see Table I). In (a) anti-phase boundaries (APB) due to steps in the $SrTiO_3$ substrate are shown (see arrows). The dotted line corresponds to a Burgers path with a Burgers vector $\mathbf{b}=[001]$ associated to it. By counting the number of layers along the Burgers path (dotted line) displayed in (b), the existence of a Burgers vector with $\mathbf{b}=[001]$ becomes apparent. This dislocation was observed in close proximity to an impurity (*A*). For a better resolution of the (001) fringes, the TEM cross section shown in (b) was laterally compressed by a factor 3.

Figure 6(b) displays another dislocation with Burgers vector $\mathbf{b}=[001]$. In order to improve the contrast of the (001) fringes, the film was tilted about 10° out of the [100] orientation such that the [001] was still perpendicular to the electron beam. In addition, the TEM micrograph in Fig. 6(b) was laterally compressed by a factor of 3. As in Fig. 6(a), the dotted line corresponds to a Burgers path with a different number of unit-cell layers to the left and right sides. In Fig. 6(b), however, the dislocation was found to be in close proximity to an impurity phase.

Finally, the general waviness of the unit-cell high layers in Fig. 6(b) is due to the intercalation of material such as additional, e.g., Ba-O or Cu-O layers. Similar defects have also been observed on Y123.[33–37] In the case of our film, there are strong indications from TEM and XRD (see the next section) that most of the intercalated layers were introduced *after film growth was completed* (e.g., by an aging effect or TEM sample preparation). As a consequence, they do not affect the growth mechanisms to be discussed later.

### 3. *X-ray diffraction*

In order to reach a comprehensive understanding of the growth of Sm123 films, XRD was performed on film JY (see Table I), the same film whose surface and cross section were investigated using STM and TEM, respectively (see Figs. 4–6). In particular the rocking curves ($\omega$ scans) of the (001) reflection of Sm123 were measured in the directions parallel and perpendicular to the step edges of the substrate (i.e., perpendicular and parallel to the miscut direction of the substrate). For more accuracy, equal statistic (1000 counts) was used for each point of the scans. The full width at half maximum (FWHM) was found to be equal to 0.16(5)° when measured parallel to the step edges and 0.31(5)° when measured perpendicular to them. Various effects can be responsible for the broadening of a rocking curve, for instance, (i) a spreading of the direction in which the crystallographic *c* axis is pointing or (ii) a reduced (lateral) size of crystallites. The two effects can be differentiated by measuring the rocking curves of higher-order reflections: for a spreading of the direction of the *c* axis, the angular linewidth would remain constant, while for a crystallite size effect, the rocking curve would be much thinner. As a consequence $\omega$ scans of the (005) and (007) reflections of Sm123 were performed (both parallel and perpendicular to the step edges). It was found that a crystallite-size effect could be neglected. Therefore, the difference in linewidths for the rocking curves of the (001) reflection indicates that there is more tilting of the *c* axis (i.e., more bending of Sm123 layers) perpendicular to the step edges than parallel to them.

Finally, it should be emphasized that the FWHM of the measured rocking curves are comparable to the values obtained by others on "good-quality" laser-ablated or sputtered Y123 films. The imperfect growth observed on our films is therefore not specific to Sm123 or the use of a codeposition technique for film fabrication.

### C. Discussion

The STM, TEM, and XRD results presented in this section indicate that the bending of Sm123 (001) layers is a characteristic property of the growth of *c*-axis-oriented Sm123. It seems likely that the substantial shearing deformation observed in Sm123 layers can be related to the structural integrity of the (strongly bonded) $CuO_2$ layers. In addition, the ledge growth[18] of Y123 and related materials allows unit-cell layers of Sm123 to "flow" over obstacles. Our experimental results provide strong evidence that these two inherent properties of Sm123 (and Y123) are responsible for the formation of screw dislocations in the presence of impurities.

A model to explain the formation of screw dislocations on our films is shown in Fig. 7. The proposed model is based on the fact that impurity phases do inhibit the flow of advancing growth fronts [Fig. 7(a)]. The experimental evidence for this pinning of growth fronts is provided by STM imaging of our films. As film growth proceeds [Fig. 7(b)], an impurity can eventually be covered by a Sm123 layer. This results in a typical bending of the Sm123 layer, in agreement with the STM results of Fig. 4(b) and the TEM result of Fig. 6(a). Further growth leads to the coalescence of two vertically misaligned growth fronts, resulting in the formation of a screw dislocation [Fig. 7(c)]. The observation by TEM of a dislocation with Burgers vector $\mathbf{b}=[001]$ in close proximity to an impurity [see Fig. 6(b)] is consistent with Fig. 7(c). Within our model, a different number of Sm123 layers are expected on both sides of the impurity associated to the screw dislocation. This was indeed observed experimentally by STM (see Fig. 5). Due to the step-flow mode in which the film in Fig 7 is grown, no spiral-shaped island will ever emanate from this screw dislocation. However, the hole, which corresponds to the core of the dislocation, has the shape of a spiral.

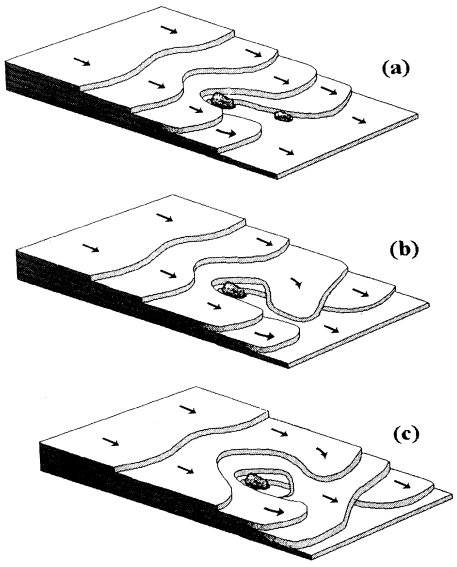


FIG. 7. Model proposed to explain structures as the one displayed in Fig. 5. The screw dislocations resulting from the meeting of vertically misaligned growth fronts do not lead to the formation of spiral-shaped islands due to step-flow growth of the film.

More generally, the impurity-related pinning of growth fronts and bending of Sm123 layers could also account for the formation of screw dislocations on *c*-axis-oriented Sm123 films grown on substrates with no or small miscut angle. In an analogous way to what is shown in Fig. 7, impurity phases could be responsible for the pinning and bending of different growth fronts, resulting in the formation of screw dislocations. However, in the case of *c*-axis-oriented Sm123 films grown on substrates with no or small miscut angle, spiral-shaped islands will emanate from these screw dislocations, resulting in an enhanced growth in vertical direction[38] and a dramatic change in surface morphology.

For completeness, it should be mentioned that our results do not rule out the possible formation of screw dislocations by inheritance from the substrate or by means of dislocation half-loops (see Sec. IV A).

## V. Sm123 GROWING WITH THE *c* AXIS PARALLEL TO THE SUBSTRATE

Depending on the conditions under which films were grown, a varying amount of Sm123 grains with their crystallographic *c* axis parallel to the surface of the substrate was observed. As these $c\parallel$ grains can strongly influence the physical (superconducting) properties of a film, the mechanisms responsible for their formation were investigated in more detail.

### A. Experimental results

#### *1. Characterization of $c\parallel$ grains*

When imaged by SEM or STM, the surface of a film containing $c\parallel$ grains (e.g., film GS, see Table I) is characterized by thin, elongated slabs growing at 90° to each other (Fig. 8). Figure 9 shows a cross-sectional TEM measurement of the same film as in Fig. 8. The dark lines correspond to planes perpendicular to the crystallographic *c* axis of Sm123. A striking characteristic of the $c\parallel$ grains is that besides being thin and long, they are also rather tall, as compared to the average thickness of the film which is 150 nm. This characteristic of the grains is emphasized by a "shadow effect" taking place during film growth and resulting in a film thickness of less than 150 nm in between narrowly spaced $c\parallel$ grains. Note that, while the STM image in Fig. 8 seems to indicate a full coverage of the film surface by $c\parallel$ grains, the TEM results of Fig. 9 clearly show that $c\perp$ regions exist in between the slabs. This discrepancy can be explained by the fact that due to its lateral dimensions, a STM tip will usually not be able to scan the regions in between two $c\parallel$ slabs. The same grains of $c\parallel$ material will most probably be imaged by various laterally and vertically shifted minitips. The shape of $c\parallel$ grains (thin along the *c* axis, long perpendicular to it), which have also been observed for Y123 (see, e.g., Refs. 27 and 39–41), results from an anisotropy in

growth speeds parallel and perpendicular to the crystallographic $c$ axis of the studied superconductor. Because the growth speed parallel to the $c$ axis is much lower than perpendicular to it, $c\|$ grains grow as thin, long, and tall slabs. Typical dimensions of the observed $c\|$ grains are 20–50 nm for the width, approximately 1 $\mu$m for the length, and 250 nm for the height (see, e.g., Figs. 8 and 9).

Although the shape of $c\|$ grains can be understood rather easily, it is still controversial why such grains nucleate at all in Y123 and related films. The observation of a critical thickness at which $c\perp$ growth switches to $c\|$ growth has repeatedly been reported.[26,42,43] It was suggested that the relaxation of strain due to substrate-film lattice mismatch was a possible reason for this transition. On the other hand, Pennycook *et al.*[12] argued that the formation of $c\|$ grains is favored at high supersaturation because their growth requires less surface diffusion. Obviously, the question whether thermodynamic or kinetic factors govern the formation of $c\|$ grains is still open. In order to reach a better understanding of the mechanisms responsible for the creation of $c\|$ grains on Sm123 films, the influence of deposition parameters such as substrate temperature, chamber pressure, and composition of the film were analyzed in more detail.

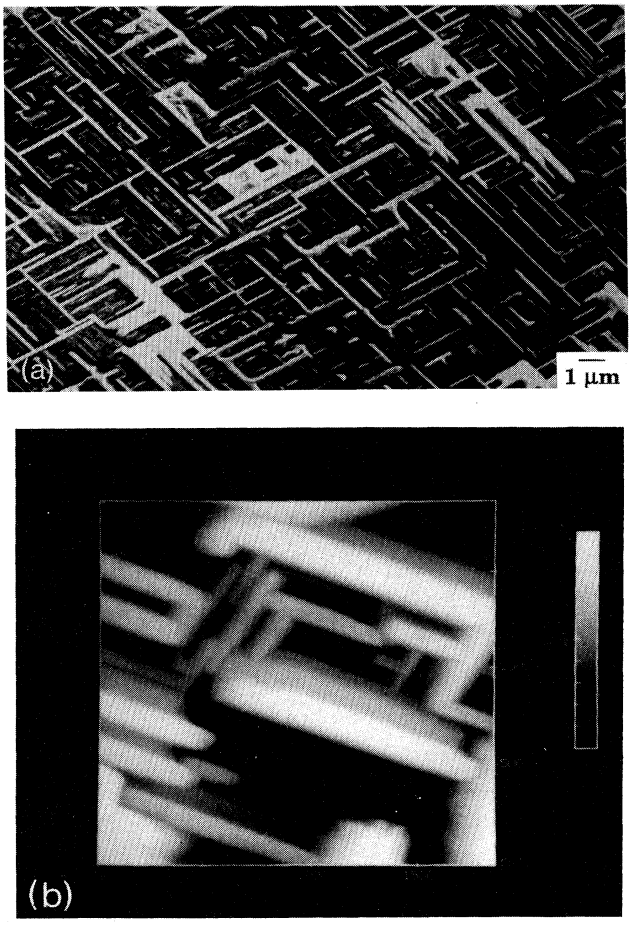


FIG. 8. (a) SEM and (b) STM micrographs of the same Sm123 film (film GS, see Table I). The surface of this film seems to be covered by thin and elongated $c\|$ grains.

### 2. *Effect of substrate temperature and chamber pressure*

In a first step, the role played by the substrate temperature $T_{sub}$ and the chamber pressure $p$ was investigated by measuring the volume fraction of $c\|$ to $c\perp$ material, using x-ray diffraction, in a series of films grown under different conditions. A four-circle diffractometer was used to measure the rocking curves of the (104) reflections of Sm123 on each film, for both the $c\|$ and $c\perp$ oriented grains. The volume fraction of $c\|$ to $c\perp$ material was then extracted by forming the ratio of the integrated intensities of these rocking curves.

The results of these measurements are displayed in Fig. 10, where the volume fraction of $c\|$ to $c\perp$ material is plotted as a function of substrate temperature $T_{sub}$. The full dots correspond to a series of films all having a compara-

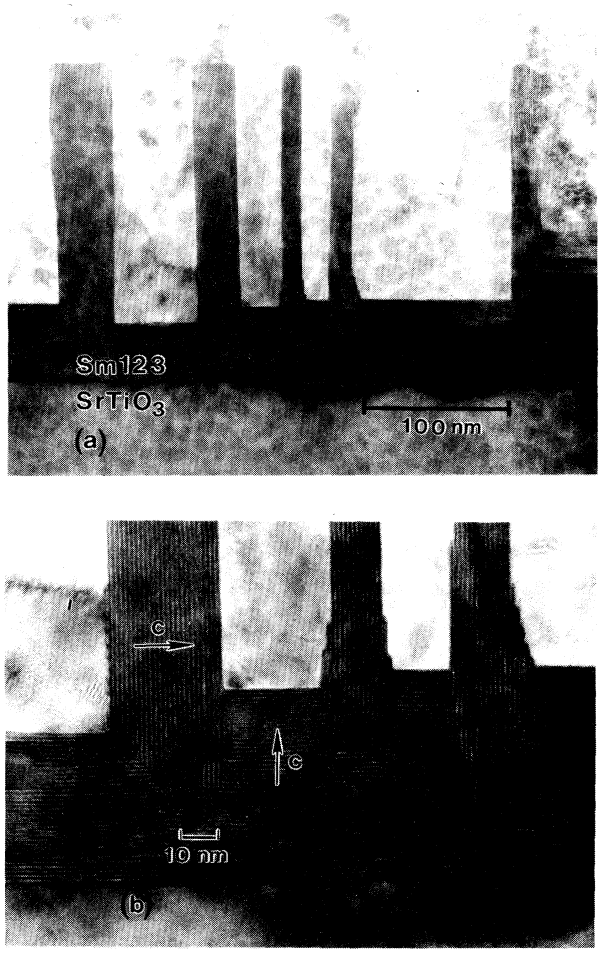


FIG. 9. (a) TEM cross-sectional view of the Sm123 film whose surface is shown in Fig. 10 (film GS, see Table I). The $c\|$ grains are not only thin and long but also rather tall. Note that the surface of the film is not fully covered by $c\|$ grains but that regions exist in between the slabs. (b) Enlarged view of (a). The dark lines correspond to planes perpendicular to the $c$ axis of Sm123.

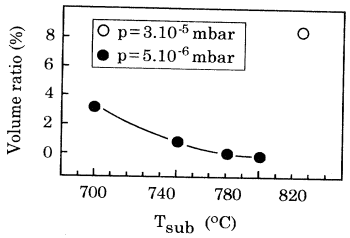


FIG. 10. Volume ratio of $c\|$ to $c\perp$ material as a function of substrate temperature $T_{sub}$ for two different chamber pressures $p$. The line is a guide to the eye. The errors are of the size of the dots or smaller.

ble Cu content (between 47 and 50%), similar vicinal angles ($\alpha=0.35°-0.65°$) and grown at a chamber pressure of $5\times10^{-6}$ mbar (films II, KA, HV, HR, see Table I). Although these films have slightly different Sm and Ba contents, this was not found to be relevant for the volume fraction of $c\|$ to $c\perp$ material. The open dot refers to a film grown at a somewhat higher pressure of $3\times10^{-5}$ mbar (film GS, see Table I). The error bars for these measurements are of the size of the dots or less. It should be mentioned here that the values plotted in Fig. 10 correspond to upper limits of the volume fractions of $c\|$ to $c\perp$ material in each film, since a geometrical correction factor of the order of 0.75 was neglected here. This factor is introduced by the different angles at which the incoming x-ray beam hits the sample when measuring the (104) reflection for the $c\|$ and the $c\perp$ material, respectively. Because the value of 0.75 is only a rough estimate based on geometrical reasoning, we prefer to display the "raw," uncorrected data in Fig. 10. As can be seen from this figure, the largest volume fraction of $c\|$ to $c\perp$ material is only 8.5(1)% and corresponds to the film whose surface and cross section are shown in Figs. 8 and 9. Films grown at $5\times10^{-6}$ mbar and at a substrate temperature of 780 °C or higher were found to have an almost vanishing amount of $c\|$ material [0.10(5)% for $T_{sub}=780$ °C, 0.0(5)% for $T_{sub}=800$ °C].

These results confirm that, as already stated in Sec. IV, the films investigated in this study are predominantly oriented with their $c$ axis perpendicular to the substrate. In addition, Fig. 10 clearly shows that the relative amount of $c\|$ material present in a film rapidly increases for decreasing $T_{sub}$ and for increasing chamber pressure $p$.

### 3. *Effect of Cu content*

A rather surprising experimental finding of this study on codeposited Sm123 films is that the surfaces of Cu-deficient films seem to be smoother, i.e., to have less outgrowths. Figure 11 displays the scanning electron micrographs of the surface of three films grown under comparable conditions ($T_{sub}=800$ °C, $p=5\times10^{-6}$ mbar) but having different Cu contents. Given as a percentage of the total amount of metallic ions deposited onto the films, these Cu contents are 52(1)% for the film in Fig. 11(a) (film JY, see Table I), 49(1)% for Fig. 11(b) (film HL) and 46(1)% for Fig. 11(c) (film HI). Figure 11 clearly shows that the density of outgrowths decreases with decreasing Cu content of the film.

From TEM measurements it is known that the droplets with irregular shape surrounding most of the outgrowths are Cu based, most probably CuO.[7] A further result of TEM measurements is that these Cu-based droplets are seen on the surface and not as inclusions in the bulk of the Sm123 films. This is in accordance with Refs. 44 and 45. Most probably, the CuO droplets have a large interface energy with Sm123. As a consequence, they are not wetting and "float" on the surface of the film during deposition. However, when they encounter an outgrowth with which they have lower interface energies, they will tend to stick to them. This explains the surface structures observed by SEM for films grown with a Cu content of 52(1) and 49(1)% [Figs. 11(a) and 11(b)]. Based on

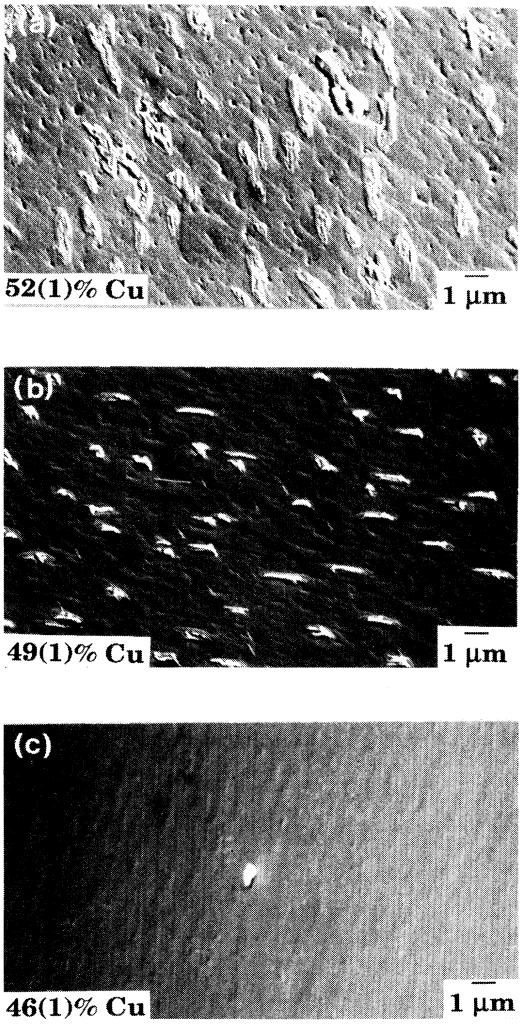


FIG. 11. Typical SEM micrographs of three Sm123 films grown with different Cu content. The Cu contents in percentage of the total amount of deposited metal ions is (a) 52(1)% (film JY, see Table I), (b) 49(1)% (film HL), and (c) 46(1)% (film HI). Note that the density of elongated slabs decreases with decreasing Cu content.

these observations, one would expect that films with a lower Cu content would still display a comparable amount of outgrowths, but without the CuO droplets sticking around them. However, it was observed experimentally that for a film grown with a Cu content of only 46(1)%, not only had the CuO droplets disappeared, but also most of the outgrowths ($c\|$ grains as well as impurity phases), resulting in the smoothest surface of all the Sm123 films investigated so far [Fig. 11(c)]. In order to test the reproducibility of this observation, a second set of films (films GV, HR, and HB, see Table I) grown (independently) under similar conditions as the films described above, was also imaged by SEM, yielding consistent results to those shown in Fig. 11. Note that no quantitative comparison between the volume fraction of $c\|$ grains and the Cu content of these films was possible, because for all six films the ratio of $c\|$ to $c\perp$ material was less than the resolution limit of 0.1% of the x-ray measurements (compare also with the data plotted in Fig. 10).

Based on the experimental evidence shown in Fig. 11, one should consider the possibility that CuO droplets are, to some extent, responsible for the formation of $c\|$ grains. However, it is at this stage not clear how such a mechanism would work.

### B. Discussion

In what follows, three possible mechanisms for the formation of $c\|$ grains will be discussed. The formation of $c\|$ grains could (1) be induced by the stress due to substrate-film lattice mismatch, (2) result from a lowered surface mobility during film growth, or (3) be triggered by second phases.

#### *1. Role of strain due to substrate-film lattice mismatch*

As suggested in Refs. 26, 42, and 43, the relaxation of strain due to the substrate-film lattice mismatch could be a driving mechanisms for the formation of $c\|$ grains. Indeed, at the temperature at which Sm123 films are grown, the substrate-film lattice mismatch is such that $c\perp$ growth on $SrTiO_3$ is accompanied by tensile stress while $c\|$ growth displays compressive stress.[46] However, the volume fractions of $c\|$ to $c\perp$ material present in our films are much too small and the distances between $c\|$ grains much too large to ensure an effective strain relaxation. Although a transition from $c\perp$ to $c\|$ growth (at a critical thickness which in literature varies between 40 and 400 nm) has repeatedly been reported,[26,42,43] our films do not display a comparable feature. Even in the case of film GS, where STM micrographs seem to show a "full surface coverage" by $c\|$ grains [see Fig. 8(b)] and x-ray diffraction reveals that the volume ratio $c\|$ to $c\perp$ is only of 8.5(1)%, the TEM results of Fig. 8 clearly show the absence of a crossover from $c\perp$ to $c\|$ growth (see also *characterization of $c\|$ grains*).

#### *2. Role of surface kinetics*

In the thermodynamic limit, the system must overcome a potential barrier $G_c$ in order to form a critical nucleus. This potential barrier has a height[47]

$$G_c=\frac{16\pi}{3}\frac{\Omega^2\alpha^3}{(\Delta\mu)^2}\ , \tag{3}$$

where $\Omega$ is the specific volume, $\alpha$ the surface energy, and $\Delta\mu$ the supersaturation. According to Ref. 47, this results in a nucleation rate $J$ (i.e., number of nuclei formed per unit volume per unit of time) proportional to

$$J\propto\exp(-G_c/k_BT)\ , \tag{4}$$

where $T$ is the temperature at which the film is grown.

Within this thermodynamic model, the ratio for the nucleation rates $J_{c\|}$ and $J_{c\perp}$ for $c\|$ and $c\perp$ islands, respectively, would be equal to

$$\frac{J_{c\|}}{J_{c\perp}}=K\exp[(\alpha_{c\perp}^3-\alpha_{c\|}^3)/k_BT]\ , \tag{5}$$

where $K$ is a constant, and $\alpha_{c\|}$ and $\alpha_{c\perp}$ represent the surface energies for $c\|$ and $c\perp$ material, respectively. Because the surface energy for $c\|$ material is known to be larger than for $c\perp$ material, Eq. (5) predicts an increase in the volume ratio of $c\|$ to $c\perp$ material for increasing growth temperature. This is in clear contradiction with the x-ray-diffraction results presented in Fig. 10. Obviously, the thermodynamic approach discussed here cannot explain our experimental results. It seems therefore likely that kinetic factors are important to understand the formation of $c\|$ grains.

If the mobility of diffusing species is reduced, defects (i.e., cation disorder) can be created which are frozen in as film growth proceeds. In other words, the low surface and bulk diffusion coefficients affect the ordering kinetics of the film. While in the thermodynamic limit one would expect the nucleation of a critical $c\|$ nucleus being several unit cells large, in the kinetic limit a single unit cell of $c\|$ Sm123 can be the starting point for a $c\|$ grain.

As shown in Fig. 10, the volume ratio of $c\|$ to $c\perp$ material increases rapidly as a function of decreasing temperature and increasing chamber pressure (i.e., increasing ozone flux). For comparison, in a TEM study of sputtered Y123 films grown on MgO, Svetchnikov *et al.*[48] observed an increase of $c\|$ material as a function of decreasing substrate temperature and decreasing oxygen partial pressure $p_{O_2}$.

The influence of the substrate temperature is consistent in both studies (Ref. 48 and this work), indicating that a reduction of the surface diffusion length results in a larger volume ratio of $c\|$ material.

On the other hand, the pressure dependence reported in Ref. 48 seems *a priori* to conflict with our results. However, one should keep in mind the different film deposition techniques used in both studies. Due to the reactiveness of ozone, the metallic species diffusing on our films are believed to be oxide molecules even for a relatively low chamber pressure (i.e., low ozone flux). By increasing the chamber pressure, additional oxygen atoms or molecules diffuse on the film surface, resulting in a decrease of the surface diffusion length. As for the temperature-dependent data discussed above, this reduc-

tion in surface diffusion length is coupled to an increase in the volume ratio of $c\|$ to $c\perp$ material (see Fig. 10). In the case of sputtered films, the species reaching the surface of the Y123 film are individual atoms for sufficiently low $p_{O_2}$ or oxide molecules for high $p_{O_2}$ pressure.[48] Because it is not clear how this change from atoms to molecules will influence the surface diffusion length, a direct comparison between the pressure dependence of $c\|$ grains in Ref. 48 and in the present study is not possible.

In order to characterize the surface kinetics in more detail, the diffusion coefficient $D$ was estimated from our data. Although estimates of $D$ on Y123 have been published in the past, the reported results vary over *several orders of magnitudes* (see, e.g., Refs. 11, 49, and 50). For two-dimensional isotropic diffusion, the diffusion coefficient $D$ is equal to

$$D = L_D^2/4\tau_D \ , \tag{6}$$

where $L_D$ is the surface diffusion length (see also Sec. IV A) and $\tau_D$ is the mean diffusion time.

The diffusion length $L_D$ can be inferred from the crossover of step-flow growth to island growth. From our STM results, we know that at 800 °C $L_D$ must be of the order of 105 nm or slightly larger.

The diffusion time $\tau_D$ must be much smaller than the time needed to deposit one unit-cell layer of Sm123 (otherwise, the film would be amorphous). A growth rate of 1 Å/s therefore yields $\tau_D \ll 12$ s, and by means of Eq. (6), $D \gg 2\times10^{-12}$ cm$^2$/s. A comparable value is reported in Ref. 49, where the recovery time $\tau \approx 10$ s of the RHEED specular beam was used to calculate the diffusion coefficient $D$. As this recovery time $\tau$ per definition was measured with zero flux of incoming atoms, it too is an upper limit for $\tau_D$.

A more accurate estimate for $\tau_D$ is obtained by assuming that atoms (or molecules) diffusing on the surface of the film undergo only few collisions before being incorporated into the bulk of the film. In this case,

$$\phi L_D^2 \tau_D \sim 1 \ , \tag{7}$$

where $\phi$ is the flux of incoming atoms. For a growth rate of 1 Å/s, the flux of incoming metal atoms is $\phi = 1.6\times10^{14}$ cm$^{-2}$s$^{-1}$. The ozone flux ($10^{16}$ cm$^{-2}$s$^{-1}$) is neglected in what follows, as it is assumed that at low chamber pressure, the effect of ozone is just to oxidize the metal atoms. Equations (6) and (7) then yield $D \sim 5\times10^{-7}$ cm$^2$/s. This result is in good agreement with estimates of the diffusion coefficients for Y ($10^{-9}$ cm$^2$/s at 800 °C) and Ba ($10^{-7}$ cm$^2$/s at 800 °C) on the surface of Y123, as reported in Ref. 50.

The diffusion coefficient $D$ is known to be equal to

$$D = a^2 v \exp(-E_s/k_B T_{sub}) \ , \tag{8}$$

where $a$ is the diffusion jump length, $v$ the jump frequency, and $E_s$ the activation energy for surface diffusion. Using the measured value of $T_{sub} = 800$ °C and assuming that $a \approx 4$ Å and $v \approx 10^{13}$ Hz, the activation energy $E_s$ was calculated to be 0.96 eV, within our model.

Finally, the temperature dependence of the volume ratio $V$ of $c\|$ to $c\perp$ material (see Fig. 10) was found to be well described by an Arrhenius law, i.e., $V \propto \exp(E/k_B T_{sub})$ with $E = 3.3(9)$ eV. Although only three points were used for this fit (samples II, KA, and HV), the above function yields a substrate temperature $T_{sub} \sim 620$ °C for a fully $c\|$ oriented film (volume ratio of 100%), which is a reasonable result.

A comparison of the temperature dependence of the diffusion coefficient $D$ and the volume ratio $V$ reveals that $V = D^{-n}$ with $n \sim 3$–4. This might reflect the fact that the energy scale related to $V$ [$E = 3.3(9)$ eV] is of the order of magnitude of activation energies for bulk diffusion. It seems therefore that a reduction of surface and/or bulk mobility results in an increase of the volume ratio of $c\|$ to $c\perp$ material. This is consistent with frozen cation disorder being the mechanism for the formation of $c\|$ grains.

### 3. *Role of second phases*

It was observed in this study that the presence of CuO droplets on the surface of the films might be related to the nucleation of $c\|$ grains. In Ref. 39, Chang *et al.* report that the dislocation configuration at triple points (the hole where three grain boundaries meet) nucleates Cu-oxide growth, which in turn nucleates $c\|$ growth. The authors emphasize that for the samples of their study, the Cu-oxide phase nucleated before formation of the $c\|$ grains.

It is at present not clear how the presence of CuO droplets could influence the formation of $c\|$ grains. However, from the results presented in this section, it is known that kinetic factors play a substantial role for the formation of $c\|$ material. One might therefore speculate,

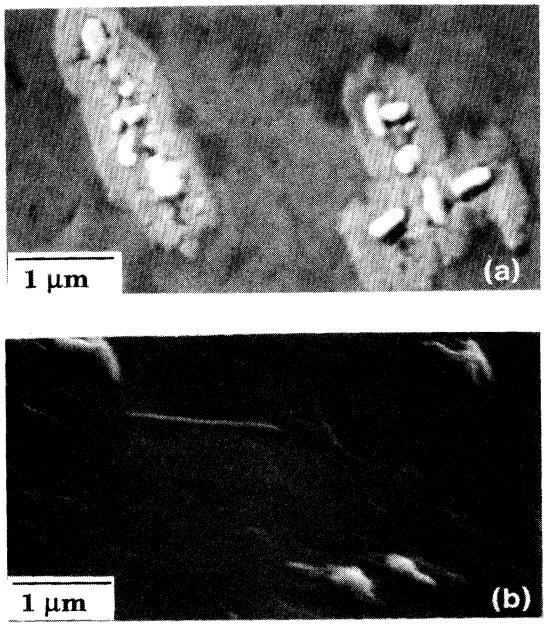


FIG. 12. SEM micrographs showing outgrowths with qualitatively different shapes. (a) Accumulation of various small tabular outgrowths (film GV, see Table I). (b) Thin and long slabs, probably $c\|$ grains (film HL).

that the CuO droplets, which "float" on the surface of the film during deposition, can locally reduce the mobility of the species which are diffusing on this same surface (for instance, by burying them in between the CuO droplets and the Sm123 film).

On the other hand, by varying the Cu content of a film, the nature, density, and distribution of other second phases within the bulk of the film are likely to be changed. Therefore, the Cu content of a film could indirectly influence the formation of $c\|$ grains at second phases other than the CuO droplets.

## VI. IMPURITY PHASES

All the Sm123 films studied here displayed a variety of impurity phases, either in the form of outgrowths on the surface or as inclusions in the bulk of the films. As discussed earlier (see Secs. IV and V), such second phases can considerably influence the morphology of the Sm123 structure.

When imaged by SEM, the surfaces of most Sm123 films display outgrowths of rather elongated shape, growing along a ⟨100⟩ direction. *A priori,* one could think that all these outgrowths correspond to Sm123 with its $c$ axis parallel to the substrate. However, a closer examination of the SEM images reveals that the observed outgrowths have quite different structures (see Fig. 12) indicating that, most probably, they are not all the same material. Furthermore, the surfaces of some films display a rather regular coverage by elongated outgrowths, but, at the same time, their volume fraction of $c\|$ to $c\perp$ material is almost vanishing. In other words, most of the elongated structures parallel to a ⟨100⟩ direction of $SrTiO_3$ do not necessarily correspond to $c\|$ grains of Sm123, but can be impurity phases growing with an epitaxial relationship to the substrate. This is in agreement with Ref. 40 where tabular outgrowths other than $c\|$ grains (e.g., $Y_2O_3$ and $YCuO_2$) were observed on Y123 films. Using cross-sectional TEM, outgrowths such as, e.g., $Sm_2CuO_4$, with a large amount of CuO surrounding them, are observed on our films. As an example, a TEM micrograph displaying two outgrowths on a Sm123 film (film HL) is shown in Fig. 13. The outgrowths are either pure $Sm_2CuO_4$ or a mixture of Sm123 and $Sm_2CuO_4$ (see Fig. 13). In contrast to the Y-Ba-Cu-O phase diagram which does not contain the $Y_2CuO_4$ phase, $Sm_2CuO_4$ is a stable phase under our growth conditions. In addition, Fig. 13 also shows that the surface of the film surrounding the outgrowth is covered by CuO.

The presence of CuO droplets on the surface of our films was already mentioned in Sec. V. TEM measurements show that these droplets never appear in the bulk of Sm123, but usually stick to other outgrowths at the surface of the film, indicating a large interface energy between them and the surrounding Sm123. As the absolute composition for each element in the Sm123 films is known within approximately 1%, it is quite certain that most of the investigated films were not Cu rich. Therefore kinetic factors were important for the creation of these droplets, since thermodynamically one would not expect CuO formation.

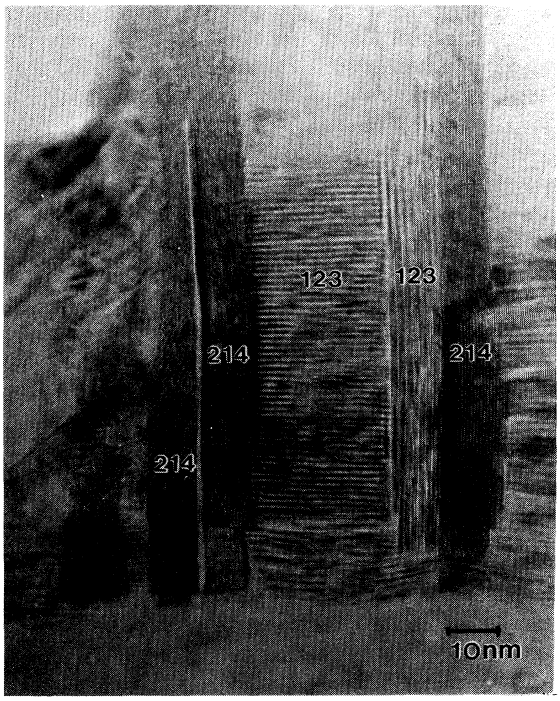


FIG. 13. TEM cross-sectional view showing two $Sm_2CuO_4$ (214) outgrowths. One of them (to the right) grows adjacent to a Sm123 (123) $c\|$ grain. Both outgrowth are surrounded by CuO. (Film HL, see Table I.)

Finally, TEM measurements also revealed the existence of $Sm_2O_3$ and $SmCuO_2$ in our films. As most of the films in this study are grown Sm-rich (see Table I), it is *a priori* not surprising, that practically all of them display some amount of $Sm_2O_3$ phases.

Because the ternary phase diagram of Sm, Ba, and Cu at high temperature and low pressure is not well known, it is difficult to determine what second phases should be expected, under equilibrium conditions, if Sm123 film is deposited slightly off stoichiometry. If we use the Y-Ba-Cu-O diagram as a reference[51] then the presence of large amounts of CuO in copper-deficient films as well as the existence of $Sm_2O_3$ inclusions are not expected from a thermodynamic point of view. This suggests that kinetic factors are also important to understand the nature of the second phases present in coevaporated Sm123 films.

## VII. CONCLUSIONS

The Sm123 films investigated here were all predominantly $c$-axis oriented with small fractions of $c\|$ grains and some impurity phases. It was found that Sm123 growing with a $c\perp$ orientation displayed a frequent bending of its unit-cell thick layers. Our STM and TEM results suggest that this bending can be related to the presence of second phases and that it can lead to the formation of screw dislocations in our films.

Sm123 grains with a $c\|$ orientation were observed on

most of our films. Based on the results presented here, it is likely that a reducted mobility of the adsorbed species during film deposition is responsible for the formation of Sm123 with its $c$ axis parallel to the substrate. In particular, the volume fraction of $c\|$ to $c\perp$ material was measured to increase with decreasing substrate temperature and increasing chamber pressure. Furthermore, our SEM results suggest that the nucleation probability of $c\|$ grains is increased if CuO droplets are present on the surface of the films. Depending on the exact composition of the investigated Sm123 films, CuO, $Sm_2O_3$, $SmCuO_2$, and $Sm_2CuO_4$ were observed.

Both thermodynamic and kinetic factors are clearly important to understand the nucleation and growth of the films investigated in this study. Our Sm123 films are all predominantly $c$-axis oriented, which in terms of surface energy is the thermodynamically preferred orientation. However, the study presented here suggests that kinetic factors do considerably influence the morphology of our films.

Indeed, we found strong evidence that the impurity-related bending of the Sm123 lattice combined with the ledge growth of the Sm123 (001) layers is responsible for the formation of screw dislocations on our films. It was observed that the impurity phases, which can lead to the formation of such dislocations, are in general unexpected from a thermodynamic point of view. Kinetic factors were therefore important for their creation. Furthermore, the formation and growth of $c\|$ grains seems to be caused by a reduction of the surface and/or bulk diffusion during film growth.

Based on the results presented here, the smoothest and most homogeneous $RBa_2Cu_3O_y$ ($R$ = Y or lanthanide) films are expected to grow under conditions which favor a high surface mobility (large diffusion coefficient) of the species during film deposition. In the case of films grown by coevaporation in ozone, this is equivalent to high substrate temperatures, low chamber pressures, and low deposition rates.

## ACKNOWLEDGMENTS

We are very grateful to H. M. Appelboom, B. Dam, T. Frey, J. P. Locquet, J. Mannhart, C. Rossel, and E. J. Williams for helpful and stimulating discussions leading to this work. We would also like to thank J. W. J. Kerssemakers and A. H. N. de Groot for their AFM micrographs and A. J. Steinfort and E. J. Sonneveld for their help in characterizing the films by means of x-ray diffraction. One of us (B.S.-P.) acknowledges financial support from DIMES. This work was supported by FOM and the Dutch National Research Program (NOP) for High-$T_c$ Superconductors.

*Present address: Department of Physics, The Norwegian Institute of Technology, University of Trondheim, N-7034 Trondheim, Norway.

†Present address: ISTEC, 10-13 Shinonome 1-chome, Koto-ku, Tokio 135, Japan.

[1]See, for instance, *Proceedings of the Fourth International Conference on Materials and Mechanisms of Superconductivity, High-Temperature Superconductors,* Grenoble, France, 1994 [Physica C **235-240** (1994)].

[2]H. M. Appelboom, Ph.D. thesis, Delft University of Technology, Delft, The Netherlands, 1991.

[3]H. M. Appelboom, V. C. Matijasevic, F. Mathu, G. Rietveld, B. Anczykowski, W. J. A. M. Peterse, F. Tuinstra, J. E. Mooij, W. G. Sloof, H. A. Rijken, S. S. Klein, and L. J. van IJzendoorn, Physica C **214**, 323 (1993).

[4]V. C. Matijasevic, H. M. Appelboom, F. Mathu, P. Hadley, D. v. d. Marel, and J. E. Mooij, IEEE Trans. Appl. Supercond. **3**, 1524 (1993).

[5]AKZO International Research GmBH, Ibbenbüren, Germany.

[6]J. G. Wen, C. Traeholt, and H. W. Zandbergen, Physica C **205**, 354 (1993).

[7]J. P. Locquet, Y. Jaccard, Ch. Gerber, and E. Mächler, Appl. Phys. Lett. **63**, 1426 (1993).

[8]J. P. Locquet, A. Catana, E. Mächler, Ch. Gerber, and J. G. Bednorz, Appl. Phys. Lett. **64**, 372 (1994).

[9]Digital Instruments, Santa Barbara, California, USA.

[10]C. Traeholt, J. G. Wen, V. Svetchnikov, A. Delsing, and H. W. Zandbergen, Physica C **206**, 318 (1993).

[11]D. G. Schlom, D. Anselmetti, J. G. Bednorz, R. F. Broom, A. Catana, T. Frey, Ch. Gerber, H.-J. Güntherodt, and J. Mannhart, Z. Phys. B **86**, 163 (1992).

[12]S. J. Pennycook, M. F. Chisholm, D. E. Jesson, R. Feenstra, S. Zhu, X. Y. Zheng, and D. J. Lowndes, Physica C **202**, 1 (1992).

[13]V. C. Matijasevic, B. Ilge, B. Stäuble-Pümpin, G. Rietveld, F. Tuinstra, and J. E. Mooij (unpublished).

[14]B. Stäuble-Pümpin, B. Ilge, V. C. Matijasevic, F. Tuinstra, and J. E. Mooij (unpublished).

[15]A. Baronnet, J. Cryst. Growth **19**, 193 (1973).

[16]D. G. Schlom, D. Anselmetti, J. G. Bednorz, C. Gerber, and J. Mannhart, J. Cryst. Growth **137**, 259 (1994).

[17]M. G. Norton and C. B. Carter, J. Cryst. Growth **110**, 641 (1991).

[18]S. K. Streiffer, B. M. Lairson, C. B. Eom, B. M. Clemens, J. C. Bravman, and T. H. Geballe, Phys. Rev. B **43**, 13 007 (1991).

[19]M. G. Norton and C. B. Carter, in *Interfaces in High-$T_c$ Superconducting Systems,* edited by S. L. Shindé and D. A. Rudman (Springer-Verlag, New York, 1994), p. 1, and references therein.

[20]R. Hull and J. C. Bean, Crit. Rev. Solid State Mater. Sci. **17**, 507 (1992), and references therein.

[21]H. Ledbetter and M. Lei, J. Mater. Res. **6**, 2253 (1991).

[22]M. Aindow and M. Yeadon, Philos. Mag. Lett. **70**, 47 (1994).

[23]X.-Y. Zheng, D. H. Lowndes, S. Zhu, J. D. Budai, and R. J. Warmack, Phys. Rev. B **45**, 7584 (1992).

[24]C. Gerber, D. Anselmetti, J. G. Bednorz, J. Mannhart, and D. G. Schlom, Nature **350**, 279 (1991).

[25]M. Hawley, I. D. Raistrick, J. G. Beery, and R. J. Houlton, Science **251**, 1587 (1991).

[26]M. E. Hawley, I. D. Raistrick, R. J. Houlton, F. H. Garzon, and M. Piza, Ultramicroscopy **42-44**, 705 (1992).

[27]I. D. Raistrick and M. Hawley, in *Interfaces in High-$T_c$ Superconducting Systems,* (Ref. 19), p. 28, and references therein.

[28]D. P. Norton, D. H. Lowndes, X.-Y. Zheng, S. Zhu, and R. J. Warmack, Phys. Rev. B **44**, 9760 (1991).

[29]H. P. Lang, H. Haefke, G. Leemann, and H.-J. Güntherodt, Physica C **194**, 81 (1992).
[30]U. Geyer, Ph.D. thesis, Georg-August Universität Göttingen, Göttingen, FRG, 1992.
[31]D. Chambonnet, D. Keller, A. Gervais, C. Fages, S. Degoy, and C. Belouet, Physica C **235-240**, 625 (1994).
[32]J. P. Hirth and J. Lothe, *Theory of Dislocations* (Wiley-Interscience, New York, 1982).
[33]R. Ramesh, D. M. Hwang, J. B. Barner, L. Nazar, T. S. Ravi, A. Inam, B. Dutta, X. D. Wu, and T. Venkatesan, J. Mater. Res. **5**, 704 (1990).
[34]M. Fendorf, C. P. Burmester, L. T. Wille, and R. Gronsky, Appl. Phys. Lett. **57**, 2481 (1990).
[35]R. Ramesh, A. Inam, T. Sands, and C. T. Rogers, Mater. Sci. Eng. B **14**, 188 (1992).
[36]R. Ramesh, C. C. Chang, T. S. Ravi, D.M. Hwang, A. Inam, X. X. Xi, X. D. Wu, and T. Venkatesan, Appl. Phys. Lett. **57**, 1064 (1990).
[37]A. F. Marshall and R. Ramesh, in *Interfaces in High-$T_c$ Superconducting Systems* (Ref. 19), p. 71, and references therein.
[38]W. K. Burton, N. Cabrera, and F. C. Frank, Philos. Trans. R. Soc. London, Ser. A **243**, 299 (1951).
[39]C. C. Chang, X. D. Wu, R. Ramesh, X. X. Xi, T. S. Ravi, T. Venkatesan, D. M. Hwang, R. E. Muenchausen, S. Foltyn, and N. S. Nogar, Appl. Phys. Lett. **57**, 1814 (1990).
[40]A. Catana, J. G. Bednorz, Ch. Gerber, J. Mannhart, and D. G. Schlom, Appl. Phys. Lett. **63**, 553 (1993).
[41]M. G. Norton, R. R. Biggers, I. Maartense, E. K. Moser, and J. L. Brown, Physica C **233**, 321 (1994).
[42]A. H. Carim, S. N. Basu, and R. E. Muenchausen, Appl. Phys. Lett. **58**, 871 (1991).
[43]J. Q. Zheng, M. C. Shih, S. Williams, S. J. Lee, H. Kajiyama, X. K. Wang, Z. Zhao, K. Viani, S. Jacobson, P. Dutta, R. P. H. Chang, J. B. Ketterson, T. Roberts, R.T. Kampwirth, and K. E. Gray, Appl. Phys. Lett. **59**, 231 (1991).
[44]T. I. Selinder, U. Helmersson, Z. Han, J.-E. Sundgren, H. Sjöström, and L. R. Wallenberg, Physica C **202**, 69 (1992).
[45]L. R. Wallenberg, T. I. Selinder, Z. Han, and U. Helmersson, Micron Microsc. Acta **23**, 231 (1992).
[46]E. Olsson and S. L. Shindé, in *Interfaces in High-$T_c$ Superconducting Systems* (Ref. 19), Fig. 4.1, p. 120.
[47]A. A. Chernov, *Modern Crystallography III, Crystal Growth* (Springer-Verlag, Berlin, 1984).
[48]V. Svetchnikov, A. Shapovalov, V. Pan, C. Traeholt, and H. W. Zandbergen (unpublished).
[49]T. Frey, C. C. Chi, C. C. Tsuei, T. Shaw, and F. Bozso, Phys. Rev. B **49**, 3483 (1994).
[50]R. E. Somekh and Z. H. Barber, in *Physics and Materials Science of High Temperature Superconductors II,* Vol. 209 of *NATO Advanced Study Institute Series E: Applied Sciences,* edited by R. Kossowsky, B. Raveau, D. Wohlleben, and S. K. Patapis (Kluwer Academic, Dordrecht, 1992), p. 443.
[51]R. Beyers and B. T. Ahn, Rev. Mater. Sci. **21**, 335 (1991).

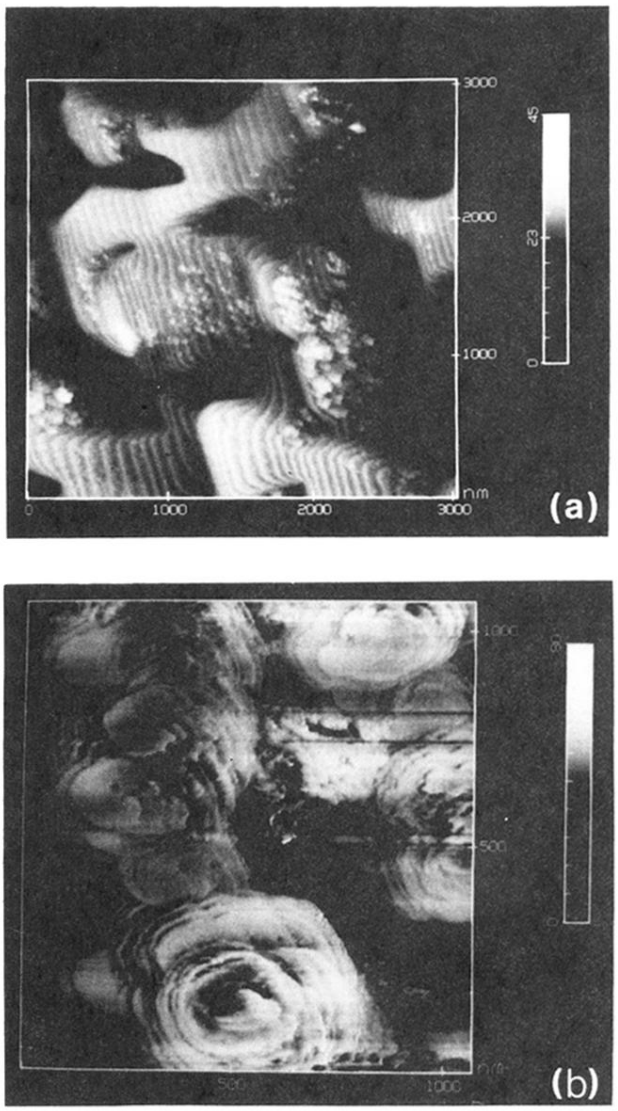


FIG. 1. STM images of coevaporated Sm123 films grown on $SrTiO_3$ showing a surface morphology characterized by (a) an apparently infinite superposition of terraces (film JY, see Table I) and (b) spiral-shaped islands (film IX).

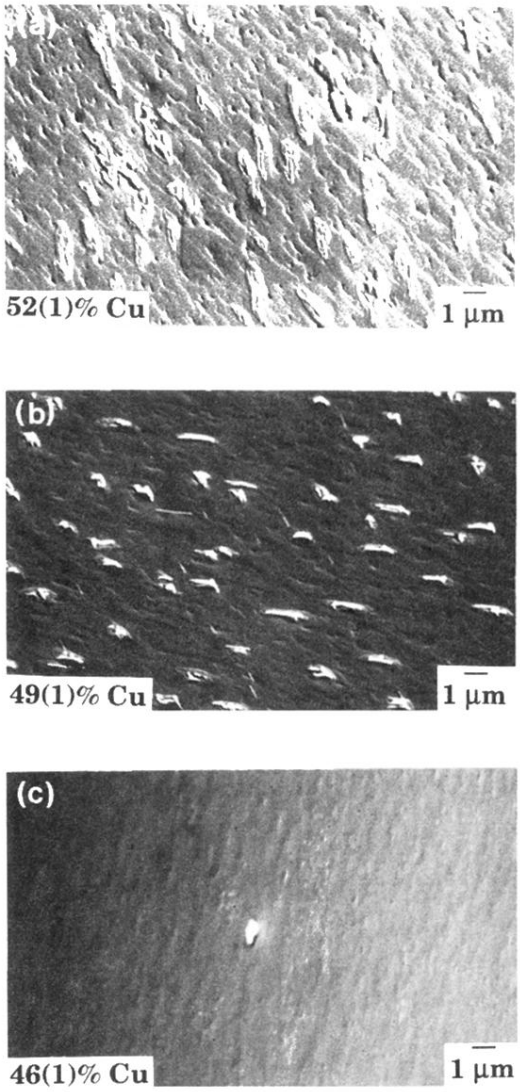


FIG. 11. Typical SEM micrographs of three Sm123 films grown with different Cu content. The Cu contents in percentage of the total amount of deposited metal ions is (a) 52(1)% (film JY, see Table I), (b) 49(1)% (film HL), and (c) 46(1)% (film HI). Note that the density of elongated slabs decreases with decreasing Cu content.

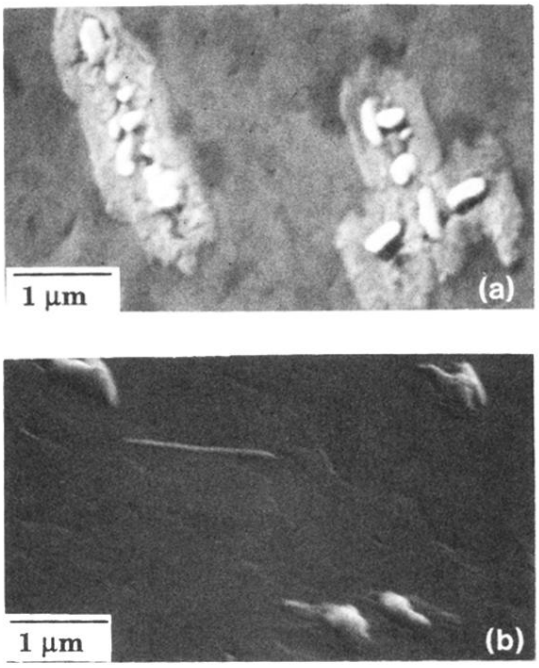


FIG. 12. SEM micrographs showing outgrowths with qualitatively different shapes. (a) Accumulation of various small tabular outgrowths (film GV, see Table I). (b) Thin and long slabs, probably $c\|$ grains (film HL).

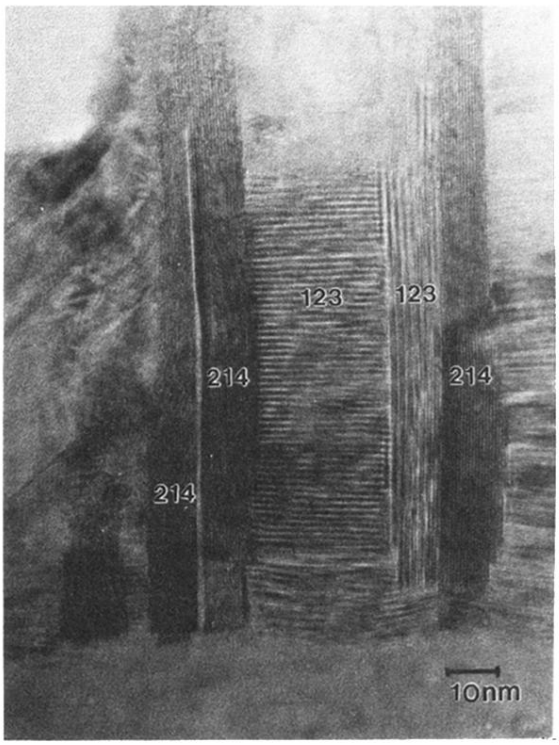


FIG. 13. TEM cross-sectional view showing two $Sm_2CuO_4$ (214) outgrowths. One of them (to the right) grows adjacent to a Sm123 (123) $c\|$ grain. Both outgrowth are surrounded by CuO. (Film HL, see Table I.)

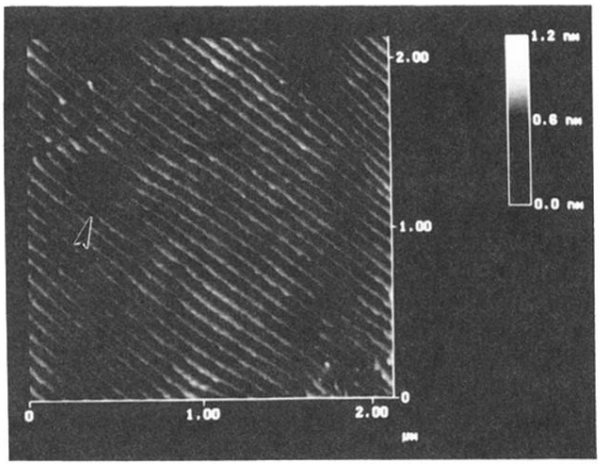


FIG. 2. AFM image of a $SrTiO_3$ substrate. The arrow points at a (screw) dislocation.

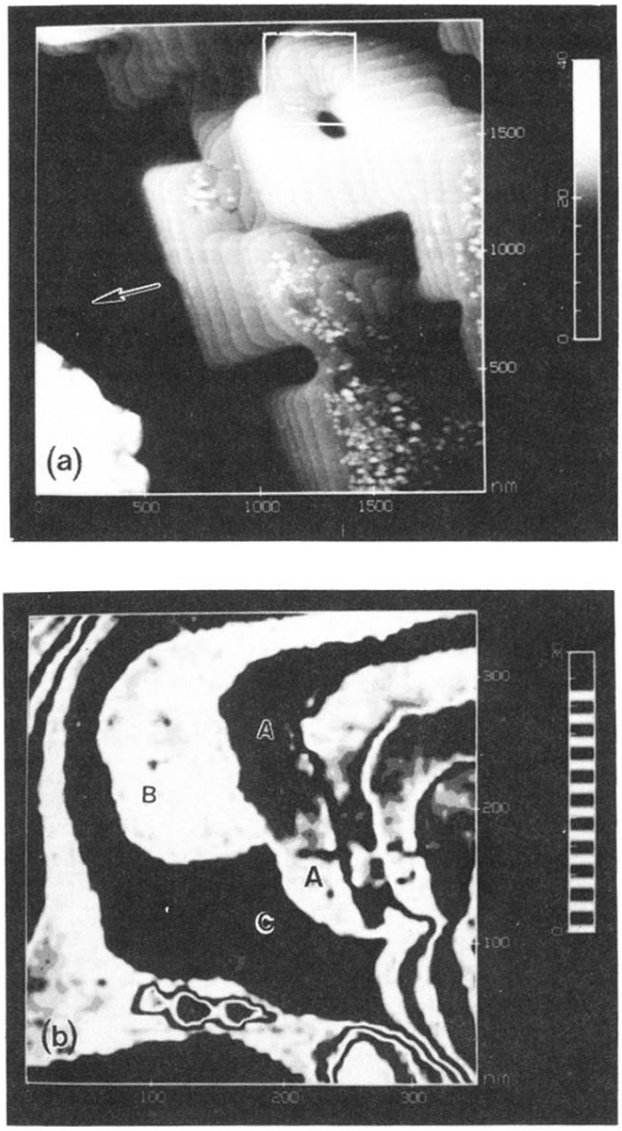


FIG. 4. (a) Typical STM image of a coevaporated Sm123 film (sample JY, see Table I) grown in the step-flow mode. The arrow roughly shows the direction toward which the substrate is miscut (see text for more details). (b) Enlarged area of (a) showing a unit-cell thick layer of Sm123 (layer *A*) bending over two other unit-cell thick layers of the same material (layers *B* and *C*). The grey scale in the *z* direction was chosen to emphasize the tilting of layer *A*.

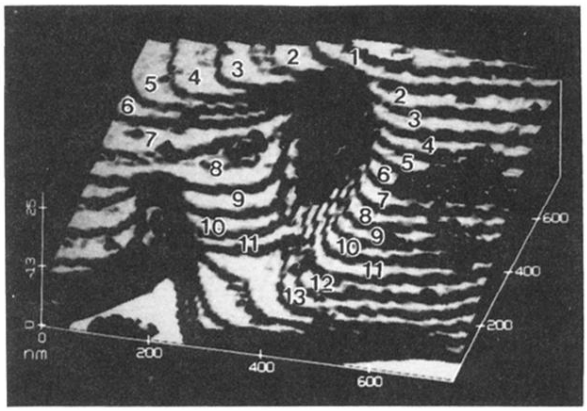


FIG. 5. STM micrograph of a Sm123 film growth in the step-flow mode (film JY, see Table I). Note that the amount of numbered terraces, all unit-cell high, is different on the left and right side of the "hole."

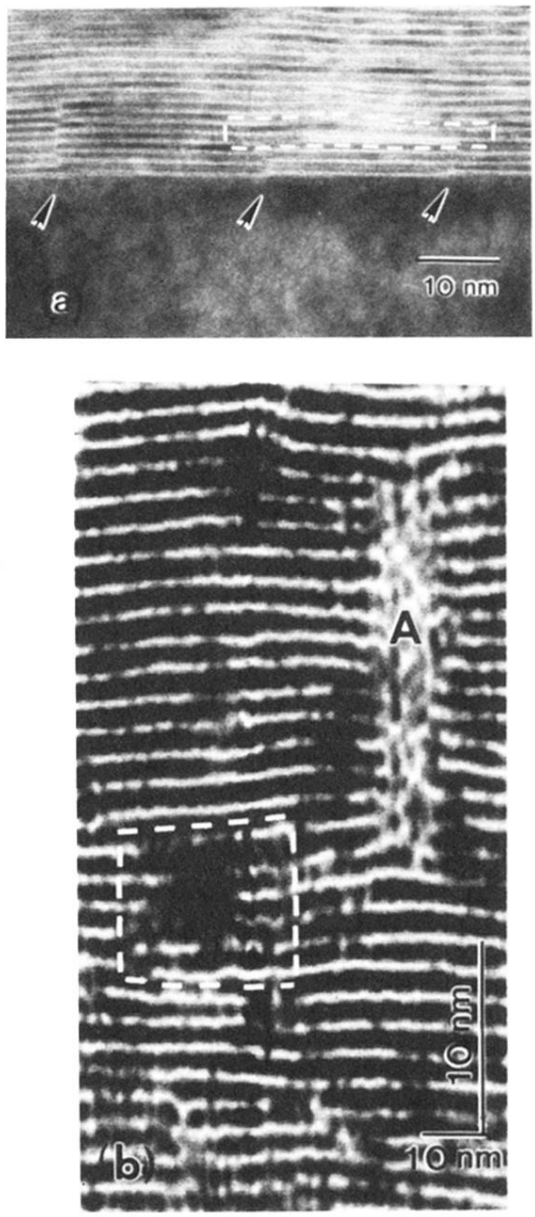


FIG. 6. TEM cross-sectional view of the Sm123 film whose surface is shown in Figs. 4 and 5 (film JY, see Table I). In (a) anti-phase boundaries (APB) due to steps in the $SrTiO_3$ substrate are shown (see arrows). The dotted line corresponds to a Burgers path with a Burgers vector $\mathbf{b}=[001]$ associated to it. By counting the number of layers along the Burgers path (dotted line) displayed in (b), the existence of a Burgers vector with $\mathbf{b}=[001]$ becomes apparent. This dislocation was observed in close proximity to an impurity ( *A* ). For a better resolution of the (001) fringes, the TEM cross section shown in (b) was laterally compressed by a factor 3.

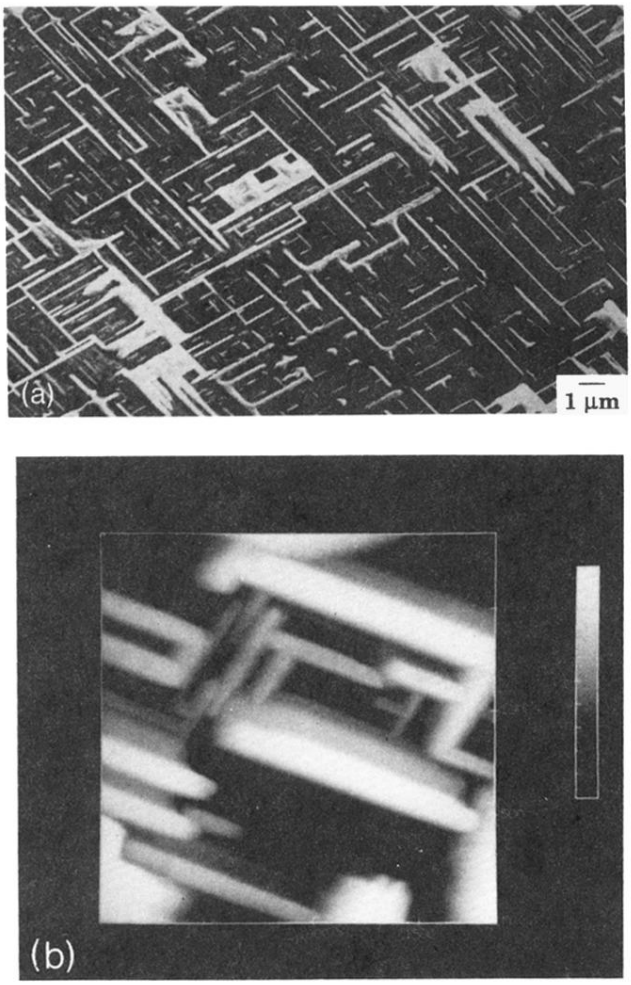


FIG. 8. (a) SEM and (b) STM micrographs of the same Sm123 film (film GS, see Table I). The surface of this film seems to be covered by thin and elongated $c\|$ grains.

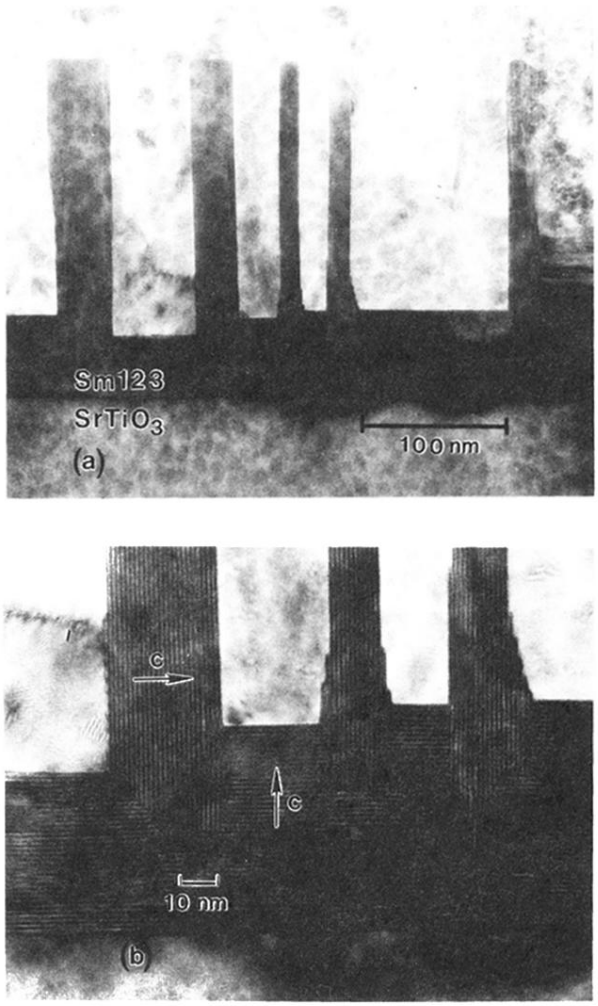


FIG. 9. (a) TEM cross-sectional view of the Sm123 film whose surface is shown in Fig. 10 (film GS, see Table I). The $c\|$ grains are not only thin and long but also rather tall. Note that the surface of the film is not fully covered by $c\|$ grains but that regions exist in between the slabs. (b) Enlarged view of (a). The dark lines correspond to planes perpendicular to the $c$ axis of Sm123.